Measurement report: Size-resolved mass concentration of equivalent black carbon-containing particle larger than 700 nm and its role in radiation

Weilun Zhao[1], Ying Li[2,3], Gang Zhao[4], Song Guo[4], Nan Ma[5], Shuya Hu[4], Chunsheng Zhao[1]

[1]Department of Atmospheric and Oceanic Sciences, School of Physics, Peking University, Beijing 100871, China

[2]Department of Ocean Science and Engineering, Southern University of Science and Technology, Shenzhen 518055, China

[3]Southern Marine Science and Engineering Guangdong Laboratory, Guangzhou 511458, China

[4]State Key Joint Laboratory of Environmental Simulation and Pollution Control, College of Environmental Sciences and Engineering, Peking University, Beijing 100871, China

[5]Institute for Environmental and Climate Research, Jinan University, Guangzhou 511443, China

Correspondence to: Chunsheng Zhao (zcs@pku.edu.cn)

Abstract. Black carbon (BC) mass size distribution (BCMSD) is crucial in both environment and climate system due to BC's intense size-dependent absorption of solar radiation. BC-containing particles of size larger than 700 nm ($BC_{>700}$) could contribute to larger than half of bulk BC mass concentration. Unfortunately, previous methods concentrated on BC-containing particles less than 700 nm because of technical limitation. The contribution of BC to absorption and radiative effect could be underestimated without consideration of $BC_{>700}$. In this study, equivalent BCMSD (eBCMSD) from 150 nm up to 1.5 μm was measured at high time resolution of 1 h for the first time by an aerodynamic aerosol classifier in tandem with an aethalometer in two field campaigns over eastern China, namely Changzhou located in the Yangtze River Delta and Beijing located in the North China Plain. The results revealed that the pattern of eBCMSD in Changzhou (Beijing) was mostly bimodal (unimodal) peaking at 240 and 1249 nm (427 nm). The peak diameter of eBCMSD in Changzhou did not shift significantly with increasing pollution (240 to 289 nm). In contrast, the peak diameter of eBCMSD in Beijing shifted towards larger size from 347 to 527 nm with increasing pollution, indicating the aging process in urban site was different from that in regional background site. eBCMSD in both Changzhou and Beijing had significant diurnal cycle with smaller (bigger) value of eBCMSD during daytime (nighttime). Equivalent $BC_{>700}$ ($eBC_{>700}$) was ubiquitous and varied significantly with different locations and pollution levels. The campaign-averaged contribution of $eBC_{>700}$ to bulk eBC mass concentration ($m_{eBC,bulk}$), bulk absorption coefficient ($\sigma_{ab,bulk}$) as well as estimated direct radiative forcing of eBC (DRF_{eBC}) in Changzhou and Beijing were 27.8 (20.9 ~ 36.5) % and 24.1 (17.5 ~ 34.2) %, 19.6 (15.8 ~ 24.6) % and 25.9 (19.6 ~ 33.7) %, as well as 20.5 (18.4 ~ 22.2) % and 21.0 (16.3 ~ 26.1) %, respectively. $m_{eBC,bulk}$, $\sigma_{ab,bulk}$ as well as DRF_{eBC} of $eBC_{>700}$ in Changzhou (Beijing) varied by 3.6 (5.1) times from 0.11 (0.07) to 0.40 (0.36) μg m^{-3}, 3.2 (5.5) times from 0.54 (0.63) to 1.75 (3.45) Mm^{-1} as well as 2.4 (4.7) times from 0.1 (0.1) to 0.24 (0.47) W m^{-2}, respectively, with the aggravation of pollution. The contribution of $eBC_{>700}$ to $m_{eBC,bulk}$ and $\sigma_{ab,bulk}$ had significant diurnal cycle with higher (lower) fraction during daytime (nighttime) in both Changzhou and Beijing.

A case study indicated that the contribution of $eBC_{>700}$ to $m_{eBC,bulk}$, $\sigma_{ab,bulk}$ and DRF_{eBC} could reach up to 50 %, 50 % and 40 %, respectively. It was highly recommended to consider whole size range of BC-containing particles in the model estimation of BC radiative effect.

1 Introduction

Black carbon (BC) is the strong light-absorbing carbonaceous particle (Bond and Bergstrom, 2006) from incomplete combustion of fossil fuel or biomass (Bond et al., 2004). Absorption of BC reduces atmospheric visibility (Moosmuller et al., 2009) and has warming effect on the climate system (Bond, 2001). BC radiative effect had considerable uncertainties. Estimated BC radiative effects from different models did not even converge to same order of magnitude (Bond et al., 2013;Szopa et al., 2021).

Previous estimation of BC radiative effect was based on bulk BC mass concentration ($m_{BC,bulk}$) from emission inventory and prescribed mass absorption cross section (MAC) (Bond et al., 2013). Both $m_{BC,bulk}$ and MAC was influenced by BC mass size distribution (BCMSD), which was one of the BC microphysical properties. BC radiative effect was highly sensitive to BCMSD (Matsui et al., 2018), and BCMSD could result in obvious variation in aerosol radiative forcing (Zhao et al., 2019). BCMSD depended on the emission source essentially. For example, the peak diameter of freshly emitted BCMSD from fossil fuel was generally smaller than that from biomass burning (Berner et al., 1984;Artaxo et al., 1998;Schwarz et al., 2008). After BC was emitted to the ambient environment, BCMSD was influenced by aging process, during which BC optical properties underwent remarkable changes (Zhang et al., 2008). For instance, BC could be coated by other non-BC materials during atmospheric transport. The existence of non-BC coating enhanced BC absorption and this phenomenon was termed as "lensing effect" (Fuller et al., 1999). The accurate quantification of lensing effect was a critical challenge in estimating BC radiative effect (Liu et al., 2017). and the information of BCMSD was required to resolve the influence of "lensing effect" on BC radiative forcing.

Guo (2016) reported that elemental carbon (EC, Petzold et al. (2013)) containing particle larger than 2.1 μm accounted for 27.6 ~ 35.2 % of bulk EC mass concentration ($m_{EC,bulk}$). Wang et al. (2017) reported that EC-containing particle larger than 1.1 μm accounted for 40.6 ~ 65.5 % of $m_{EC,bulk}$. Wang et al. (2022) indicated EC-containing particle larger than 1 μm contributed to 50 ~ 54 % of $m_{EC,bulk}$. Therefore, BC-containing particle larger than 1 μm contributed to significant part of total BC mass. Wang et al. (2022) found that these large carbon-containing particles were super-aggerated BC particles with fractal structure or BC-containing particles with massive coating from secondary processes. Chakrabarty et al. (2014) found that the optical property of these super BC aggeragates could be significant. It should be noted that current characterization of BC-containing particle larger than 1 μm could be only achieved through offline microscopy analysis (Chakrabarty et al., 2014) or EC mass size distribution (ECMSD) measurement by off-line thermo/optical organic carbon/elemental carbon analysis of size-segregated filter-based samples (Chow et al., 2001). The resulting time-resolution of ECMSD was 24 ~ 48 h. Considering that the typical time scale of BC aging was 4 ~ 18 h (Peng et al., 2016), current measured ECMSD could not resolve

atmospheric aging of BC-containing particles larger than 1 μm. Actually, current method capable of measuring BC-containing particle on time scale of BC aging was limited to size less than 700 nm, namely laser-induced incandescence technique (Schwarz et al., 2006). The characterization of BC-containing particles larger than 700 nm ($BC_{>700}$) during atmospheric aging was still unclear. The contribution of $BC_{>700}$ to absorption and BC radiative forcing was lack of study.

In this study, equivalent BC (eBC, Petzold et al. (2013)) mass size distribution (eBCMSD) up to 1.5 μm was measured with a time resolution of 1 h to study the evolution of equivalent $BC_{>700}$ ($eBC_{>700}$) as well as the contribution of $eBC_{>700}$ to bulk eBC mass concentration ($m_{eBC,bulk}$), bulk absorption coefficient ($\sigma_{ab,bulk}$) and eBC direct radiative forcing. The size referred to the particle size, not the BC core size, in this study. eBCMSD was determined by an aerosol aerodynamic classifier (AAC, Cambustion, UK, Tavakoli and Olfert (2013)) in tandem with an aethalometer (model AE33, Magee, USA, Drinovec et al. (2015), AAC – AE33) based on the method proposed by Zhao et al. (2022). eBCMSD was measured in two different locations of eastern China to study the spatial difference of $eBC_{>700}$. Direct radiative forcing of eBC (DRF_{eBC}) was estimated by the Santa Barbara DISORT (discrete ordinates radiative transfer) Atmospheric Radiative Transfer (SBDART) model (Ricchiazzi et al., 1998).

The structure of this study was organized as follows. Section 2 introduced the field measurement, instrumental setup, and details about estimation of DRF_{eBC}. Section 3 discussed the evolution as well as mass, absorption and radiation contribution of $eBC_{>700}$ based on the field measurement. Section 4 came to the conclusions.

2 Methods

2.1 Field measurement

The AAC-AE33 system was first applied to a field measurement in Changzhou, Jiangsu Province, China (119°36′E, 31°43′N), situated at the Yangtze River Delta, from May 17th to June 3rd in 2021 (Summer). Changzhou was between two meta cities, namely Nanjing (82 km to the northwest) and Shanghai (187 km to the southeast). There were no emission sources around the measurement site in Changzhou. Thus, pollution around the site was dominated by regional transportation and the measurement site in Changzhou was a typical regional background site (Zhao et al., 2022).

Then, the AAC-AE33 was deployed in Beijing, China (116°18′E, 39°59′N), located in the North China Plain, from October 29th 2021 to January 25th 2022 (Winter). The measurement site was near 2 busy streets, namely Zhongguancun Street to the west and Chengfu Road to the south. Therefore, the measurement site in Beijing was representative of urban environment Zhao et al. (2019).

2.2 Instrumental setup

The instrumental setup for eBCMSD measurement was illustrated in detail by Zhao et al. (2022) and introduced here briefly. As shown in Fig. 1, a PM_{10} inlet (16.67 L min^{-1}) was used to sample ambient aerosol particles. Then particles passed through a silica gel diffusion drier, where relative humidity (RH) was decreased to less than 30 %, before sampled by the AAC-AE33. AAC-AE33 measured size-resolved absorption coefficient ($\sigma_{ab,size-resolved}$) at a flow rate of 3 L min^{-1} in Changzhou and 2 L

96 min⁻¹ in Beijing, respectively. AAC was set to scan 12 logarithmically equally distributed aerodynamic sizes ranging from

97 200 nm to 1.5 μm in Changzhou and 150 nm to 1.5 μm in Beijing, respectively. It should be pointed out that particle diameter

98 (D_p) was aerodynamic size in this study. Particles of each scanned size were sampled for 5 min, so the time resolution of

99 $\sigma_{ab,size\text{-}resolved}$ came to 1 h. The measured $\sigma_{ab,size\text{-}resolved}$ at wavelength of 880 nm by AE33 was used to derive eBCMSD because

100 BC was the major contributor of aerosol absorption at 880 nm (Ramachandran and Rajesh, 2007).

101 The principle of retrieving σ_{ab} from AE33 was proposed by Hansen et al. (1984) and described here briefly. Aerosol-laden

102 flow with flow rate of F flew into AE33, where the aerosol particles were collected on a region with area of S of a filter. The

103 filter was illuminated by light sources at specific wavelengths. Part of the light transmitted through the particle-laden (particle-

104 free) area of the filter and the transmitted light intensity was denoted as I (I_0). The light attenuation ATN was defined as

105 $$\text{ATN} = -100 \cdot \ln\left(\frac{I}{I_0}\right). \tag{1}$$

106 Assume ATN changed by ΔATN in time interval of Δt, the attenuation coefficient σ_{ATN} was defined as

107 $$\sigma_{ATN} = \frac{S}{100 \cdot F} \cdot \frac{\Delta\text{ATN}}{\Delta t}. \tag{2}$$

108 The light attenuation was actually caused by both absorption of paticles and scattering of particles as well as the filter, which

109 was called multi-scattering effect. The multi-scattering effect was corrected based on the study of Zhao et al. (2020), where a

110 parameter $C_f = 2.9$ was introduced to derive σ_{ab}:

111 $$\sigma_{ab} = \frac{\sigma_{ATN}}{C_f}. \tag{3}$$

112 Besides multi-scattering effect, loading effect was also required to be corrected, namely, the change in ATN was not linearly

113 dependent on aerosol loading. Drinovec et al. (2015) developed "dual-spot" technique to correct loading effect, which was

114 adopted by this study.

115 MAC was required to convert absorption coefficient to eBC mass concentration. The size-dependent MAC was modeled

116 based on the scheme proposed by Zhao et al. (2021) at wavelength of 880 nm, which required size-resolved particle number

117 concentration ($N_{size\text{-}resolved}$). Concisely, took 700nm of D_p as an example, the number fraction of BC-containing particle (f_{BC})

118 was assumed a fixed parameter (0.35), and the number concentration of BC-containing particle (N_{BC}) at D_p of 700 nm could

119 be derived by

120 $$N_{BC} = f_{BC} \cdot N_{size\text{-}resolved} \cdot \Delta\log D_p, \tag{4}$$

121 where $\Delta\log D_p$ was the logarithmic width of the D_p size bin. The fixed-f_{BC} assumption led to ∼ 3 % uncertainty in derived m_{eBC}.

122 We assumed that all BC-containing particles at D_p of 700 nm had the same core size D_{BC}. An optimal D_{BC} was found so that

123 calculated absorption ($\sigma_{ab,calc}$) matched measured absorption ($\sigma_{ab,meas}$), namely

124 $$\sigma_{ab,calc} = \rho_{BC}\frac{\pi}{6}D_{BC}^3 \cdot \text{MAC}_{Mie} \cdot N_{BC} = \sigma_{size\text{-}resolved} \cdot \Delta\log D_p = \sigma_{ab,meas}, \tag{5}$$

125 where ρ_{BC} was density of BC and assumed to be a fixed value (1.8 g cm⁻³), MAC_{Mie} was Mie-calculated MAC at D_p of 700

nm and the optimal D_{BC}. eBCMSD at D_p of 700 nm could be calculated by

$$\text{eBCMSD}_{Dp=700nm} = \frac{\sigma_{ab,size-resolved}}{\text{MAC}_{Mie}}. \tag{6}$$

The assumption on the MAC led to ~ 24 % uncertainty on derived m_{eBC}. It should be noted that dust was not considered in this study. $N_{size-resolved}$ was measured by a scanning mobility particle sizer (SMPS, TSI, USA) at 0.3 L min^{-1} as well as an aerodynamic particle sizer (APS, TSI, USA) at 5 L min^{-1} in Changzhou and an AAC in tandem with condensation particle counter (CPC, TSI, USA, AAC – CPC, Johnson et al. (2018)) at 1 L min^{-1} in Beijing, respectively. AAC-AE33 measured $\sigma_{ab,size-resolved}$ and determined eBCMSD synchronously. Therefore, the contribution of eBC$_{>700}$ to both bulk absorption and $m_{eBC,bulk}$ could be quantified simultaneously.

In this study, the bulk mass concentration of eBC-containing particle ($m_{eBC,bulk}$) was defined as

$$m_{eBC,bulk} = \int_{200\,nm}^{1500\,nm} \frac{dm_{eBC}}{dlogD_p} dlogD_p, \tag{7}$$

where $\frac{dm_{eBC}}{dlogD_p}$ was eBCMSD, and the lower limit of integral was 200 nm in both Changzhou and Beijing for the convenience of comparison. The bulk mass concentration of eBC$_{>700}$ ($m_{eBC,bulk,>700}$) was defined as

$$m_{eBC,bulk,>700} = \int_{700\,nm}^{1500\,nm} \frac{dm_{eBC}}{dlogD_p} dlogD_p. \tag{8}$$

The contribution of eBC$_{>700}$ to $m_{eBC,bulk}$ ($f_{m,>700}$) was defined as

$$f_{m,>700} = \frac{m_{eBC,bulk,>700}}{m_{eBC,bulk}} \times 100\ \%. \tag{9}$$

It should be noted that BC-containing particle of D_p lower than 200 nm and greater than 1500 nm was not considered in this study, which leads to discrepancy between true $f_{m,>700}$ ($\hat{f}_{m,>700}$) and estimated $f_{m,>700}$. By simple mathematical analysis, it could be proofed that $\hat{f}_{m,>700}$ in the range of

$$\frac{1}{2}\left(f_{m,>700} + \frac{\int_{1500\,nm}^{+\infty} \frac{dm_{eBC}}{dlogD_p} dlogD_p}{\int_{200\,nm}^{1500\,nm} \frac{dm_{eBC}}{dlogD_p} dlogD_p} \right) < \hat{f}_{m,>700} < f_{m,>700} + \frac{\int_{1500\,nm}^{+\infty} \frac{dm_{eBC}}{dlogD_p} dlogD_p}{\int_{200\,nm}^{1500\,nm} \frac{dm_{eBC}}{dlogD_p} dlogD_p}, \tag{10}$$

where $\int_{200\,nm}^{1500\,nm} \frac{dm_{eBC}}{dlogD_p} dlogD_p$ was actually $m_{eBC,bulk,}$ in this study.

Similarly, the bulk absorption coefficient ($\sigma_{ab,bulk}$) was defined as

$$\sigma_{ab,bulk} = \int_{200\,nm}^{1500\,nm} \frac{d\sigma_{ab}}{dlogD_p} dlogD_p, \tag{11}$$

where $\frac{d\sigma_{ab}}{dlogD_p}$ was $\sigma_{ab,size-resolved}$. The bulk absorption coefficient of eBC$_{>700}$ ($\sigma_{ab,bulk,>700}$) was defined as

$$\sigma_{ab,bulk,>700} = \int_{700\,nm}^{1500\,nm} \frac{d\sigma_{ab}}{dlogD_p} dlogD_p. \tag{12}$$

The contribution of eBC$_{>700}$ to $\sigma_{ab,bulk}$ ($f_{ab,>700}$) was defined as

$$f_{ab,>700} = \frac{\sigma_{ab,bulk,>700}}{\sigma_{ab,bulk}} \times 100\ \%. \tag{13}$$

2.3 Estimation of direct radiative forcing of equivalent black carbon

The direct radiative effect was one of the BC characteristics that arouse extensive concerns. The SBDART model was employed to study the characteristics of DRF_{eBC}. Specifically, the instantaneous DRF_{eBC} was estimated at the top of atmosphere (TOA) under the cloud-free condition. Wavelengths from 250 nm to 4 μm were simulated in this study. Direct radiative forcing of aerosol ($DRF_{aerosol}$) was defined as (Zhao et al., 2018):

$$DRF_{aerosol} = (F_{aerosol,\downarrow} - F_{aerosol,\uparrow}) - (F_{clearsky,\downarrow} - F_{clearsky,\uparrow}), \tag{14}$$

where $F_{aerosol,\downarrow}$ ($F_{aerosol,\uparrow}$) was downward (upward) radiative irradiance flux at TOA with aerosol, and $F_{clearsky,\downarrow}$ ($F_{clearsky,\uparrow}$) was downward (upward) radiative irradiance flux at TOA without aerosol. Direct radiative forcing of aerosol without eBC ($DRF_{aerosol,noneBC}$) was defined as:

$$DRF_{aerosol,noneBC} = (F_{aerosol,noneBC,\downarrow} - F_{aerosol,noneBC,\uparrow}) - (F_{clearsky,\downarrow} - F_{clearsky,\uparrow}), \tag{15}$$

where $F_{aerosol,noneBC,\downarrow}$ ($F_{aerosol,noneBC,\uparrow}$) was downward (upward) radiative irradiance flux at TOA with aerosol except eBC. The DRF_{eBC} was defined as the difference between $DRF_{aerosol}$ and $DRF_{aerosol,noneBC}$:

$$DRF_{eBC} = (F_{aerosol,\downarrow} - F_{aerosol,\uparrow}) - (F_{aerosol,noneBC,\downarrow} - F_{aerosol,noneBC,\uparrow}). \tag{16}$$

Similarly, the direct radiative forcing of $eBC_{>700}$ ($DRF_{eBC,>700}$) was defined as:

$$DRF_{eBC,>700} = (F_{aerosol,\downarrow} - F_{aerosol,\uparrow}) - (F_{aerosol,noneBC,>700,\downarrow} - F_{aerosol,noneBC,>700,\uparrow}), \tag{17}$$

where $F_{aerosol,noneBC,>700,\downarrow}$ ($F_{aerosol,noneBC,>700,\uparrow}$) was downward (upward) radiative irradiance flux at TOA with aerosol except $eBC_{>700}$. The contribution of $eBC_{>700}$ to DRF_{eBC} ($f_{DRF,>700}$) was defined as

$$f_{DRF,>700} = \frac{DRF_{eBC,>700}}{DRF_{eBC}} \times 100\ \%. \tag{18}$$

SBDART simulation required information of surface albedo, vertical profiles of meteorological parameters and aerosol optical parameters. Surface albedo was acquired from Moderate Resolution Imaging Spectroradiometer (MODIS)/Terra surface reflectance data with temporal and spatial resolution of 1 d and 0.05° (MOD09CMG). The gridded data around the measurement site was averaged to represent surface albedo of the measurement site.

The vertical profile of meteorological parameters included vertical profile of pressure, temperature, water vapor and ozone, which were obtained from the fifth generation ECMWF (European Center for Medium Range Weather Forecasts) reanalysis data for global climate and weather (ERA5). The ERA5 data had temporal and spatial resolution of 1 h and 0.25° with 38 vertical layers from surface to about 50 km above surface. At each layer, the gridded data around the measurement site was also averaged to represent meteorological parameters of the measurement site. The time resolution of meteorological parameters was averaged to daily to match that of surface albedo.

The vertical profile of aerosol optical parameters included the vertical profile of bulk aerosol extinction coefficient ($\sigma_{ext,bulk}$), single scattering albedo (SSA) and asymmetry factor (g) at different wavelengths, which were parameterized based on the study of Zhao et al. (2019) and described here briefly. The bulk aerosol particle number concentration (N_{bulk}) was parameterized according to aircraft study by Liu et al. (2009). Dry $N_{size-resolved}$ at different heights had the same shape after

184 normalized by corresponding N_{bulk}. The parameterization of $m_{eBC,bulk}$ and eBCMSD was the same as N_{bulk} and dry $N_{size\text{-}resolved}$.

185 As for mixing state, 51% of eBC mass was assumed externally mixed and the rest of eBC mass was assumed internally mixed

186 with core-shell geometry (Ma et al., 2012) in each size bin. For the case of aerosol without eBC-containing particle (larger

187 than 700 nm), eBCMSD (larger than 700 nm) was set to 0. The aerosol optical parameters varying with height-dependent RH

188 were calculated by Mie scattering theory and κ-Kohler theory (Petters and Kreidenweis, 2007) assuming hygroscopic growth

189 parameter of 0.22 (Tan et al., 2019). The refractive indices of eBC, water and non-eBC material without water were assumed

190 $1.8 + 0.54i$ (average among the wavelengths of 450, 550 and 700 nm) (Kuang et al., 2015), $1.33 + 10^{-7}i$ (wavelength of 550

191 nm) and $1.53 + 10^{-7}i$ (wavelength of 550 nm) (Wex et al., 2002), respectively. The refractive index of non-eBC material mixed

192 with water after hygroscopic growth was derived by volume-weighted rule (Wex et al., 2002). In short, real-time measured

193 eBCMSD and $N_{size\text{-}resolved}$ were used as boundary condition at ground level to construct parameterized vertical aerosol profile.

194 When calculating aerosol optical parameters at each altitude, mixing state of BC-containing particle was assumed to be the

195 same at each altitude, each time and each D_p. With the above information, the vertical profiles of $\sigma_{ext,bulk}$, SSA and g could be

196 calculated based on Mie theory. The time resolution of aerosol optical parameters was averaged to daily to match that of

197 surface albedo.

198 **3 Results and discussion**

199 **3.1 Case study**

200   A pollution episode took place from October 31st, 2021 to November 6, 2021 in Beijing, which was used for case study to

201 illustrate the large variability of $eBC_{>700}$. The geometric mean diameter ($\overline{D}_p$) of eBCMSD was defined as

202
$$\log \overline{D}_p = \frac{\int \log D_p \cdot \frac{dm_{eBC}}{d\log D_p} d\log D_p}{\int \frac{dm_{eBC}}{d\log D_p} d\log D_p}, \tag{19}$$

203 which was used to depict the spectral variation of eBCMSD because eBCMSD did not always had an explicit modal pattern

204 and the corresponding peak diameter was not always easy to be distinguished.

205   With the development of pollution, $\overline{D}_p$ shifted apparently from around 400 nm to around 600 nm (Fig. 2a). $m_{eBC,bulk}$

206 ($m_{eBC,bulk,>700}$) increased from less than 0.5 (0.15) μg m^{-3} to as large as 2.5 (1.0) μg m^{-3} by 5.0 (6.6) times. $\sigma_{ab,bulk}$ ($\sigma_{ab,bulk,>700}$)

207 increased from less than 4 (1) Mm^{-1} to as large as 25 (10) Mm^{-1} by 6.3 (10.0) times. DRF$_{eBC}$ (DRF$_{eBC,>700}$) increased from 1

208 (0.2) W m^{-2} to as large as 4 (1) W m^{-2} by 4.0 (5.0) times. It could be seen that the variability of $eBC_{>700}$ was significant. $f_{m,>700}$,

209 $f_{ab,>700}$ and $f_{DRF,>700}$ increased from about 20 %, 20 % and 20 % to as large as 50 %, 50 % and 40 %, respectively (Fig. 2b),

210 clearly showing important role of $eBC_{>700}$ in BC mass, absorption as well as radiative effect.

211 **3.2 Equivalent black carbon mass size distribution**

212 **3.2.1 Overview**

213   The timeseries of eBCMSD in Changzhou and Beijing was shown in Fig. S1a and Fig. S1b1 – S1b4. eBCMSD was

214 presented with normalized probability density function (pdf) to study general characteristics of eBCMSD. Figure 3a1 and 3a2

were the normalized pdf over the whole campaign of Changzhou and Beijing, respectively. It could be seen that eBCMSD in Changzhou was significantly different from that in Beijing. There were two modes in the median of eBCMSD in Changzhou, which peaked at around 240 nm and 1249 nm, respectively. Yu et al. (2010) found 3 modes in ECMSD, namely modes around 300 nm, 1 μm and 5 μm, and named the 3 modes as condensation mode, droplet mode and coarse mode, respectively. Following the nomenclature by Yu et al. (2010), the mode peaking at 240 nm and 1249 nm could be termed as condensation mode and droplet mode, respectively. In contrast, only condensation mode was identified in median eBCMSD in Beijing, which peaked at 427 nm. The variation of eBCMSD, defined as the difference between upper quartile and lower quartile, in Changzhou was overall smaller than that in Beijing. The variation of eBCMSD value in Changzhou (Beijing) ranged from 0.52 (0.54) μg m^{-3} to 0.91 (1.73) μg m^{-3} with average value of 0.75 (1.05) μg m^{-3}. The maximum upper quartile of eBCMSD in Changzhou was 1.58 μg m^{-3}. In comparison, the upper quartile of eBCMSD in Beijing could reached up to 2.14 μg m^{-3}, indicating the evolution of eBCMSD in Beijing was more drastic than that in Changzhou.

3.2.2 Evolution with respect to pollution level

In order to investigate the evolution of eBCMSD under different pollution stages, eBCMSD was grouped into 3 periods: (1) clean period in which $m_{eBC,bulk}$ was lower than 0.5 μg m^{-3}, (2) transitional period in which $m_{eBC,bulk}$ was greater than 0.5 μg m^{-3} but lower than 1.0 μg m^{-3}, (3) polluted period in which $m_{eBC,bulk}$ was greater than 1.0 μg m^{-3}. Data from clean, transitional and polluted period accounted for 22.6 % (30.9 %), 51.3 % (31.9 %) and 26.0 % (37.2 %) of total data in Changzhou (Beijing), respectively, showing that Changzhou (Beijing) was dominated by transitional (polluted) period in this study.

In the clean period, there was no distinct difference in eBCMSD between Changzhou (Fig. 3b1) and Beijing (Fig. 3b2). Neither eBCMSD in Changzhou nor eBCMSD in Beijing exhibited obvious modal structure in the size range of measurement. The value of eBCMSD in both Changzhou and Beijing decreased with increasing D_p in general. For Changzhou (Beijing), the median of eBCMSD decreased from 0.87 (0.47) μg m^{-3} at 200 nm to 0.26 (0.26) μg m^{-3} at 1500 nm with average value of 0.42 (0.34) μg m^{-3}. The variation of eBCMSD in Changzhou (Beijing) was 0.24 (0.24) μg m^{-3} ~ 0.47 (0.55) μg m^{-3} with average value of 0.32 (0.35) μg m^{-3}, showing that the variation of eBCMSD in Changzhou was comparable to that in Beijing.

As polluted stage evolved to transitional period, the value of eBCMSD increased in both Changzhou (Fig. 3c1) and Beijing (Fig. 3c2) compared to that in clean period. The variation of eBCMSD in Changzhou (Beijing) reached 0.41 (0.44) μg m^{-3} ~ 0.86 (0.86) μg m^{-3} with average value of 0.53 (0.61) μg m^{-3}, about twice as much as that in clean period. It could be seen that the value of median and variation of eBCMSD in Changzhou were comparable to that in Beijing. However, the pattern of eBCMSD in Changzhou was obviously different from that in Beijing. The peak value of median eBCMSD located at 240 (347) nm in Changzhou (Beijing). Median eBCMSD in Changzhou exhibited two modes, namely condensation mode and droplet, with boundary at around 866 nm. In comparison, median eBCMSD in Beijing only had one mode, namely condensation mode. It should be noted that two modes (one mode) meant that there were two distinct groups (one group) of

247 BC-containing particles with respect to D_p, not the BC core size (D_{BC}). The difference in peak diameter of condensation mode

248 between Changzhou and Beijing was as large as 107 nm. Median eBCMSD at clean period was subtracted from that at

249 transitional period to study eBC mass increment at each D_p, as shown in Fig. S4a1. It could be clearly seen that mass increment

250 in Changzhou peaked at 289 nm and 1249 nm, contributing to condensation mode and droplet mode in eBCMSD, respectively.

251 In contrast, mass increment in Beijing only peaked at 385 nm, contributing to condensation mode in eBCMSD.

252 As the pollution stage came to polluted period, the value of eBCMSD increased drastically in both Changzhou (Fig. 3d1)

253 and Beijing (Fig. 3d2) compared to that in clean period. Both the median value and the variation of eBCMSD increased with

254 the development of pollution. The median eBCMSD increased to 0.88 (0.61 ~ 2.12 (2.45) μg m^{-3} with average value of 1.49

255 (1.52) μg m^{-3} in Changzhou (Beijing), about 4 times as much as the median eBCMSD in clean period. The variation of

256 eBCMSD in Changzhou (Beijing) reached 0.60 (0.73) ~ 1.11 (1.06) μg m^{-3} with average value of 0.92 (0.94) μg m^{-3}, about 3

257 times as much as that in clean period. The difference in pattern of eBCMSD between Changzhou and Beijing became more

258 distinct. Median eBCMSD in Changzhou clearly exhibited a bimodal structure where the condensation mode and droplet

259 mode peaked at 289 nm and 1249 nm, respectively. Median eBCMSD in Beijing exhibited a unimodal structure where the

260 condensation mode peaked a 527 nm. As shown in Fig. S4b1, the peak of mass increment in Changzhou (Beijing) shifted

261 from 289 (385) nm to 347 (527) nm, varied by 58 (142) nm. The significant difference in the shift of peak indicated that aging

262 processes in regional background site was significantly different from that in urban site.

3.2.3 Contribution of equivalent black carbon-containing particle larger than 700 nm to bulk equivalent black carbon

mass concentration

265 The median (lower quartile ~ upper quartile) of $m_{eBC,bulk}$ was 0.73 (0.52 ~ 1.03) μg m^{-3} in Changzhou and 0.79 (0.43 ~ 1.31)

266 μg m^{-3} in Beijing (Fig. 4a1). The median of $m_{eBC,bulk}$ was comparable between Changzhou and Beijing. The variation of

267 $m_{eBC,bulk}$ in Changzhou, 0.51 μg m^{-3}, was smaller than that in Beijing, 0.88 μg m^{-3}. $m_{eBC,bulk,>700}$ in Changzhou was overall

268 comparable to that in Beijing (Fig. 4a2). $m_{eBC,bulk,>700}$ was 0.20 (0.13 ~ 0.32) μg m^{-3} in Changzhou and 0.18 (0.10 ~ 0.33) μg

269 m^{-3} in Beijing. Therefore, eBC$_{>700}$ was ubiquitous. Considering that the variation of $m_{eBC,bulk,>700}$ in Changzhou, 0.19 μg m^{-3},

270 was comparable to that in Beijing, 0.23 μg m^{-3}, the larger variation in $m_{eBC,bulk}$ in Beijing was mainly from eBC-containing

271 particles less than 700 nm. $f_{m,>700}$ was 27.8 (20.9 ~ 36.5) % in Changzhou and 24.1 (17.5 ~ 34.2) % in Beijing (Fig. 4a3),

272 indicating that eBC$_{>700}$ was overall one quarter of m$_{eBC,bulk}$. $f_{m,>700}$ in Changzhou was slightly larger than that in Beijing, which

273 was contributed by droplet mode of eBCMSD in Changzhou. A summary table with respect to m_{eBC} was presented in Table 1.

274 The statistics of mass contribution of eBC$_{>700}$ were studied with different pollution stages. As shown in Fig. 4a1, $m_{eBC,bulk}$

275 increased from 0.41 (0.33 ~ 0.45) μg m^{-3} in clean period through 0.71 (0.58 ~ 0.83) μg m^{-3} in transitional period to 1.33 (1.16

276 ~ 1.71) μg m^{-3} in polluted period by 3.2 times in Changzhou and increased from 0.32 (0.22 ~ 0.41) μg m^{-3} in clean period

277 through 0.73 (0.61 ~ 0.85) μg m^{-3} in transitional period to 1.47 (1.21 ~ 1.82) μg m^{-3} in polluted period by 4.6 times in Beijing.

278 As shown in Fig. 4a2, the change of $m_{eBC,bulk,>700}$ with pollution level was substantial in both Changzhou and Beijing. For

279   Changzhou, $m_{eBC,bulk,>700}$ increased from 0.11 (0.07 ~ 0.15) µg m^{-3} in clean period to 0.20 (0.14 ~ 0.27) µg m^{-3} in transition

280   period, and reached 0.40 (0.29 ~ 0.50) µg m^{-3} in polluted period, increasing by as large as 3.6 times from clean period to

281   polluted period. For Beijing, $m_{eBC,bulk,>700}$ increased from 0.07 (0.05 ~ 0.12) µg m^{-3} in clean period to 0.17 (0.11 ~ 0.23) µg

282   m^{-3} in transition period, and reached 0.36 (0.25 ~ 0.52) µg m^{-3} in polluted period, increasing by as large as 5.1 times from

283   clean period to polluted period. The change in $m_{eBC,bulk}$ and $m_{eBC,bulk,>700}$ was overall consistent with the development of

284   pollution, leading to unconspicuous change in $f_{m,>700}$ (Fig. 4a3). $f_{m,>700}$ in Changzhou changed from 28.5 (20.3 ~ 36.0) % in

285   clean period through 28.4 (20.7 ~ 36.9) % in transitional period to 27.4 (22.6 ~ 36.2) % in polluted period. $f_{m,>700}$ in Beijing

286   varied from 26.2 (18.4 ~ 36.8) % in clean period through 22.8 (16.3 ~ 32.3) % in transition period to 23.8 (18.1 ~ 31.9) %

287   in polluted period.

288   **3.2.4 Diurnal cycle**

289   It could be seen clearly that the value of eBCMSD during daytime was overall lower than that during nighttime in both

290   Changzhou (Fig. 5a1) and Beijing (Fig. 5a2), indicating that eBCMSD was regulated by planetary boundary layer or

291   difference in surface emission source (Liu et al., 2019). For Changzhou (Beijing), eBCMSD from 10:00 to 18:00 (08:00 to

292   18:00) was obviously lower that from 20:00 to 06:00 (20:00 to 06:00). Accordingly, $m_{eBC,bulk}$ in Changzhou reached minimum

293   of 0.56 (0.48 ~ 0.88) µg m^{-3} at 12:00 and maximum of 0.97 (0.80 ~ 1.24) µg m^{-3} at 21:00 (Fig. 5b1). $m_{eBC,bulk}$ in Beijing

294   reached minimum of 0.65 (0.42 ~ 1.02) µg m^{-3} at 14:00 and maximum of 1.08 (0.55 ~ 1.52) µg m^{-3} at 00:00, (Fig. 5b2). The

295   apparent diurnal cycle was found in the condensation mode of eBCMSD, which was mostly less than 700 nm. In contrast,

296   diurnal cycle was not obvious for eBCMSD larger than 700 nm for both Changzhou and Beijing. Consequently, neither

297    $m_{eBC,bulk,>700}$ in Changzhou (Fig. 5c1) nor $m_{eBC,bulk,>700}$ in Beijing (Fig. 5c2) exhibited obvious diurnal cycle. $m_{eBC,bulk,>700}$ in

298   both Changzhou and Beijing fluctuated around 0.2 µg m^{-3}, consistent with Sect. 3.2.3. Combining the diurnal variation of

299    $m_{eBC,bulk}$ and $m_{eBC,bulk,>700}$, $f_{m,>700}$ was negatively correlated to $m_{eBC,bulk}$ according to Eq. (9) with higher value during the

300   daytime and lower value during the nighttime. $f_{m,>700}$ reached maximum of 35.4 (26.6 ~ 41.1) % at 09:00 and reached

301   minimum of 23.6 (13.9 ~ 30.8) % at 21:00 in Changzhou (Fig. 5d1). $f_{m,>700}$ reached maximum of 31.0 (20.8 ~ 36.9) % at

302   15:00 and reached minimum of 23.5 (16.1 ~ 27.8) % at 01:00 in Beijing (Fig. 5d2).

303   **3.3 Size-resolved absorption coefficient**

304   **3.3.1 Overview**

305   The general characteristics (timeseries) of $\sigma_{ab,size\text{-}resolved}$ in Changzhou and Beijing was shown in Fig. 3a3 (Fig. S2a) and Fig.

306   3a4 (Fig. S2b1 – S2b4), respectively. The median $\sigma_{ab,size\text{-}resolved}$ in both Changzhou and Beijing both exhibited unimodal

307   structure. For Changzhou (Beijing), $\sigma_{ab,size\text{-}resolved}$ had maximum value of 7.88 (10.59) Mm^{-1} at 416.1 (427.2) nm and minimum

308   value of 1.63 (2.90) Mm^{-1} at 1500 (1500) nm with average value of 5.39 (6.21) Mm^{-1}. The maximum value was 4.9 (3.7)

309   times as large as minimum value in Changzhou (Beijing), showing the significant dependence of absorption on particle size.

310   D_p which had higher median value of $\sigma_{ab,size\text{-}resolved}$ corresponded to larger variation on the whole. The variation of $\sigma_{ab,size\text{-}}$

resolved ranged from 2.25 (2.82) Mm^{-1} at 1500 (1500) nm to 7.43 (17.90) Mm^{-1} at 500 (527) nm with average value of 4.99 (8.97) Mm^{-1} in Changzhou (Beijing). The variation of $\sigma_{ab,size\text{-}resolved}$ was as large as the median value of $\sigma_{ab,size\text{-}resolved}$ in both Beijing and Changzhou, showing the large variability of BC absorption. The variation of $\sigma_{ab,size\text{-}resolved}$ in Beijing was overall 1.8 times as large as that in Changzhou, indicating that the evolution of $\sigma_{ab,size\text{-}resolved}$ in different sites could be significantly different.

3.3.2 Evolution with respect to pollution level

$\sigma_{ab,size\text{-}resolved}$ was grouped into 3 periods based on $m_{eBC,bulk}$ as described in Sect. 3.2.2. In clean period, the value of $\sigma_{ab,size\text{-}resolved}$ overall decreased with increasing D_p in both Changzhou (Fig. 3b3) and Beijing (Fig. 3b4), and the pattern of $\sigma_{ab,size\text{-}resolved}$ had no obvious modal structure. In Changzhou (Beijing), the value of $\sigma_{ab,size\text{-}resolved}$ decreased from 4.67 (3.43) Mm^{-1} at 200 (427) nm to 0.88 (1.80) Mm^{-1} at 1500 (1500) nm with average value of 2.95 (2.49) Mm^{-1}. The variation of $\sigma_{ab,size\text{-}resolved}$ in Changzhou (Beijing) ranged from 1.06 (1.57) Mm^{-1} to 2.72 (3.12) Mm^{-1} with average value of 2.04 (2.47) Mm^{-1}.

During the transitional period, the unimodal pattern could be identified in both Changzhou (Fig. 3c3) and Beijing (Fig. 3c4). Median $\sigma_{ab,size\text{-}resolved}$ peaked at 416 (427) nm with value of 7.80 (10.04) Mm^{-1} in Changzhou (Beijing). Median $\sigma_{ab,size\text{-}resolved}$ in clean period was subtracted from that in transitional period to study absorption increment at each D_p, as shown in Fig. S4a2. The increment of $\sigma_{ab,size\text{-}resolved}$ in Changzhou (Beijing) had maximum value of 3.94 (6.61) Mm^{-1} at 416 (427) nm and minimum value of 0.66 (1.15) Mm^{-1} at 1500 (1500) nm. The increment of absorption was most at around 420 nm and least at 1500 nm, showing the significant difference in the change of absorption at different D_p with the development of pollution. The maximum increment of absorption in Beijing was 1.7 times as large as that in Changzhou. Hence, the evolution of absorption could be different substantially in different locations. The variation of $\sigma_{ab,size\text{-}resolved}$ in Changzhou (Beijing) ranged from 1.94 (2.32) Mm^{-1} to 4.03 (6.43) Mm^{-1} with average value of 3.08 (4.45) Mm^{-1}, increasing by about 1.5 times compared to clean period.

In the polluted period, the unimodal pattern of $\sigma_{ab,size\text{-}resolved}$ was significant in both Changzhou (Fig. 3d3) and Beijing (Fig. 3d4). Median $\sigma_{ab,size\text{-}resolved}$ peaked at 416 (527) nm with value of 16.79 (25.85) Mm^{-1} and had minimum value of 2.85 (4.23) Mm^{-1} at 1500 (1500) nm in Changzhou (Beijing). Compared to transition period, peak diameter remained unchanged in Changzhou but increased by 100 nm in Beijing, indicating the evolution of $\sigma_{ab,size\text{-}resolved}$ with aging process was different between regional background site and typical urban site. The increment of absorption in Changzhou (Beijing) was most significant at 416 (527) nm with value of 12.93 (22.94) Mm^{-1} and least at 1500 (1500) nm with value of 1.97 (2.44) Mm^{-1}, as shown in Fig. S4b2. It could be seen that the diameter of increment in absorption remain unchanged in Changzhou and shifted by 100 nm in Beijing, indicating that absorption at different D_p varied differently at different locations with the deterioration of pollution. The variation of $\sigma_{ab,size\text{-}resolved}$ in Changzhou (Beijing) ranged from 2.19 (3.82) Mm^{-1} to 9.05 (15.61) Mm^{-1} with average value of 5.72 (8.22) Mm^{-1}, increasing by about 3 times compared to clean period, indicating that the variability of $\sigma_{ab,size\text{-}resolved}$ increased with the development of pollution.

3.3.3 Contribution of equivalent black carbon-containing particle larger than 700 nm to bulk absorption coefficient

It could be seen from the timeseries of $\sigma_{ab,size\text{-}resolved}$ in both Changzhou (Fig. S2a) and Beijing (Fig. S2b1 – S2b4) that absorption of $eBC_{>700}$ was nonnegligible. $\sigma_{ab,bulk}$ was 4.93 (3.53 ~ 7.24) Mm^{-1} in Changzhou and 6.37 (3.31 ~ 11.68) Mm^{-1} in Beijing on the whole, as shown in Fig. 4b1. Both median and variation of $\sigma_{ab,bulk}$ in Changzhou were less than that in Beijing. $\sigma_{ab,bulk,>700}$ was 1.03 (0.62 ~ 1.59) Mm^{-1} in Changzhou, accounting for 19.6 (15.8 ~ 24.6) % of $\sigma_{ab,bulk}$, and 1.47 (0.81 ~ 2.83) Mm^{-1} in Beijing, accounting for 25.9 (19.6 ~ 33.7) % of $\sigma_{ab,bulk}$, respectively, as shown in Fig. 4b2 and Fig. 4b3. It could be clearly seen that $eBC_{>700}$ contributed to substantial part of total absorption, and should be explicitly considered in BC radiative estimation. A summary table with respect to σ_{ab} was presented in Table 1.

With the aggravation of pollution, the change of $m_{eBC,bulk}$ in Changzhou was overall in agreement with that in Beijing (Fig. 4a1). However, the change of $\sigma_{ab,bulk}$ with the development of pollution was different between Changzhou and Beijing (Fig. 4b1). In the clean period, $\sigma_{ab,bulk}$ in Changzhou with value of 2.71 (2.30 ~ 3.28) Mm^{-1} was comparable to that in Beijing with value of 2.47 (1.65 ~ 3.28) Mm^{-1}. In the transitional period, $\sigma_{ab,bulk}$ was 4.83 (4.04 ~ 6.02) Mm^{-1} in Changzhou and 5.93 (4.72 ~ 7.33) Mm^{-1} in Beijing. The deviation in $\sigma_{ab,bulk}$ was about 1 Mm^{-1} between Changzhou and Beijing. In the polluted period, $\sigma_{ab,bulk}$ was 9.61 (7.99 ~ 11.93) Mm^{-1} in Changzhou and 13.65 (10.94 ~ 17.59) Mm^{-1} in Beijing. The deviation in $\sigma_{ab,bulk}$ came to 4 Mm^{-1} between Changzhou and Beijing. It could be seen that with the development of pollution, the change of $\sigma_{ab,bulk}$ in Changzhou was less than that in Beijing. MAC_{bulk}, defined as the ratio of median $\sigma_{ab,bulk}$ to median $m_{eBC,bulk}$, changed from 6.61 (7.72) $m^2 g^{-1}$ through 6.80 (8.13) $m^2 g^{-1}$ to 7.23 (9.29) $m^2 g^{-1}$ in Changzhou (Beijing). The increase in MAC_{bulk} in both Changzhou and Beijing with the aggravation of pollution indicated the aging of BC. MAC_{bulk} in Changzhou was overall lower than that in Beijing and increased slower than that in Beijing with the development of pollution, indicating that the BC properties and aging process in Changzhou (regional background site) differentiate from that in Beijing (typical urban site).

$\sigma_{ab,bulk,>700}$ in both Changzhou and Beijing increased with the development of pollution, as shown in Fig. 4b2. $\sigma_{ab,bulk,>700}$ increased from 0.54 (0.62 ~ 1.59) Mm^{-1} through 0.96 (0.72 ~ 1.32) Mm^{-1} to 1.75 (1.53 ~ 2.36) Mm^{-1} in Changzhou and increased from 0.63 (0.43 ~ 0.91) Mm^{-1} through 1.36 (1.01 ~ 1.79) Mm^{-1} to 3.45 (2.46 ~ 5.34) Mm^{-1} in Beijing. $\sigma_{ab,bulk,>700}$ increased by 3.2 (5.5) times in Changzhou (Beijing). The relative increase of $\sigma_{ab,bulk,>700}$ was overall consistent with that of $\sigma_{ab,bulk}$ in both Changzhou and Beijing. As a result, there was no significant change in $f_{ab,>700}$ with the development of pollution (Fig. 4b3). $f_{ab,>700}$ varied from 19.8 (15.2 ~ 23.8) % through 19.3 (15.9 ~ 25.3) % to 19.6 (15.5 ~ 24.5) % in Changzhou and varied from 27.9 (20.7 ~ 36.4) % through 23.2 (17.8 ~ 30.7) % to 26.7 (20.4 ~ 34.7) % in Changzhou. It could be seen that the increase of $\sigma_{ab,bulk,>700}$ in Changzhou was less than that in Beijing with the development of pollution. Specifically, $\sigma_{ab,bulk,>700}$ in Beijing was 2.0 times larger than that in Changzhou, showing that the change of $\sigma_{ab,bulk,>700}$ with the aggravation of pollution could be different significantly in different sites.

3.3.4 Diurnal cycle

$\sigma_{ab,size\text{-}resolved}$ exhibited clear diurnal cycle in both Changzhou (Fig.5a3) and Beijing (Fig. 5a4) with lower value of $\sigma_{ab,size\text{-}}$

resolved during daytime and higher value during nighttime. Accordingly, $\sigma_{ab,bulk}$ had minimum value of 3.51 (3.16 ~ 4.26) Mm^{-1} at 14:00 and maximum value of 7.20 (3.80 ~ 10.58) Mm^{-1} at 01:00 in Changzhou (Fig. 5b3). $\sigma_{ab,bulk}$ had minimum value of 3.96 (2.97 ~ 9.10) Mm^{-1} at 14:00 and maximum value of 7.86 (4.04 ~ 13.19) Mm^{-1} at 00:00 in Beijing (Fig. 5b4), reflecting the regulation by planetary boundary layer. In contrast, neither $\sigma_{ab,bulk,>700}$ in Changzhou (Fig. 5c3) nor $\sigma_{ab,bulk,>700}$ in Beijing (Fig. 5c4) exhibited obvious diurnal cycle. Therefore, $f_{ab,>700}$, inversely proportional to $\sigma_{ab,bulk}$, had higher value during daytime and lower value during nighttime. For Changzhou, $f_{ab,>700}$ reached maximum at 09:00 with value of 25.3 (20.4 ~ 27.4) % and came to minimum at 21:00 with value of 16.6 (13.0 ~ 19.6) % (Fig. 5d3). For Beijing, $f_{ab,>700}$ reached maximum at 10:00 with value of 30.4 (21.1 ~ 36.3) % and came to minimum at 01:00 with value of 24.5 (17.2 ~ 28.1) % (Fig. 5d4).

3.4 Direct radiative forcing of equivalent black carbon

3.4.1 Overview

The timeseries of DRF$_{eBC}$ in Changzhou and Beijing was shown in Fig. S3a1 and Fig. S3b1 – S3b4, respectively. It could be seen that DRF$_{eBC}$ varied significantly in both Changzhou and Beijing. DRF$_{eBC}$ was estimated to be 0.93 (0.70 ~ 1.39) W m^{-2} in Changzhou and 1.10 (0.65 ~ 2.00) W m^{-2} in Beijing, respectively (Fig. 4c1). The variation of DRF$_{eBC}$ was as large as the median value of DRF$_{eBC}$, clearly indicating the large variability of BC radiative effect. DRF$_{eBC}$ increased substantially with the aggravation of pollution (Fig. 4c1). DRF$_{eBC}$ increased from 0.38 (0.38 ~ 0.38) W m^{-2} through 0.77 (0.70 ~ 0.98) W m^{-2} to 1.67 (1.29 ~ 2.07) W m^{-2} by 4.4 times in Changzhou and from 0.42 (0.33 ~ 0.66) W m^{-2} through 1.17 (0.79 ~ 1.45) W m^{-2} to 2.41 (1.68 ~ 2.86) W m^{-2} by 5.7 times in Beijing with the development of pollution. A summary table with respect to DRF$_{eBC}$ was presented in Table 1.

3.4.2 Contribution of equivalent black carbon-containing particle larger than 700 nm to direct radiative forcing of equivalent black carbon

DRF$_{eBC,>700}$ was estimated to be 0.19 (0.13 ~ 0.26) W m^{-2} in Changzhou and 0.20 (0.13 ~ 0.37) W m^{-2} in Beijing (Fig. 4c2), respectively, which accounted for 20.5 (18.4 ~ 22.2) % and 21.0 (16.3 ~ 26.1) % of DRF$_{eBC}$ (Fig. 4c3), respectively. Therefore, eBC$_{>700}$ contributed to an important portion of BC radiative effect. With the aggravation of pollution, DRF$_{eBC,>700}$ increased substantially and was different regionally (Fig. 4c2), DRF$_{eBC,>700}$ increased from 0.10 (0.10 ~ 0.10) W m^{-2} through 0.17 (0.12 ~ 0.26) W m^{-2} to 0.24 (0.22 ~ 0.30) W m^{-2} by 2.4 times in Changzhou and from 0.10 (0.08 ~ 0.12) W m^{-2} through 0.20 (0.17 ~ 0.24) W m^{-2} to 0.47 (0.34 ~ 0.71) W m^{-2} by 4.7 times in Beijing. The characteristics of $f_{DRF,>700}$ with increasing pollution was complicated (Fig. 4c3). $f_{DRF,>700}$ varied from 25.0 (25.0 ~ 25.0) % through 21.1 (20.3 ~ 22.3) % to 17.6 (15.5 ~ 18.9) % in Changzhou, exhibiting a decreasing trend. However, $f_{DRF,>700}$ varied from 24.4 (17.4 ~ 27.7) % through 18.4 (15.4 ~ 24.5) % to 21.5 (19.1 ~ 26.9) % in Changzhou, without systematical change.

4 Conclusions

Black carbon (BC) mass size distribution (BCMSD) was an important factor influencing environmental and radiative effect of BC. However, current BCMSD measurements mainly focused on BC-containing particle less than 700 nm. The

407 characters of BC-containing particle greater than 700 nm ($BC_{>700}$) remained uncertain due to limit in technique. In this

408 study, the characteristics of equivalent $BC_{>700}$ ($eBC_{>700}$) were measured and studied based on field measurements in eastern

409 China.

410 Equivalent BCMSD (eBCMSD) was measured from 150 nm up to 1.5 μm with time resolution of 1 hour based on the

411 method proposed by Zhao et al. (2022), where eBCMSD was determined by an aerodynamic aerosol classifier (AAC) in

412 tandem with an aethalometer (model AE33, AAC – AE33) and size-resolved particle number concentration was measured

413 concurrently to model the influence of particle size on mass absorption cross section (Zhao et al., 2021). AAC – AE33 was

414 applied to two field measurements in eastern China, namely Changzhou located in the Yangtze River Delta from May 17th to

415 June 3rd in 2021 and Beijing located in the North China Plain from October 29th 2021 to January 26th 2022. Changzhou was

416 a regional background site and Beijing was a typical urban site. The direct radiative forcing of eBC (DRF_{eBC}) was estimated

417 by Santa Barbara DISORT (discrete ordinates radiative transfer) atmospheric radiative transfer (SBDART) model (Ricchiazzi

418 et al., 1998).

419 eBCMSD was different between Changzhou and Beijing. Campaign-averaged eBCMSD in Changzhou exhibited two

420 modes, peaking at 240 nm and 1249 nm, respectively. In contrast, campaign-averaged eBCMSD in Beijing exhibited one

421 mode, peaking at 427 nm. $eBC_{>700}$ was ubiquitous in both Changzhou and Beijing. The campaign-averaged mass, absorption

422 as well as radiative contribution of $eBC_{>700}$ to buk eBC mass concentration ($m_{eBC,bulk}$), bulk absorption coefficient ($\sigma_{ab,bulk}$),

423 as well as DRF_{eBC} in Changzhou and Beijing were 27.8 (20.9 ~ 36.5) % and 24.1 (17.5 ~ 34.2) %, 19.6 (15.8 ~ 24.6) % and

424 25.9 (19.6 ~ 33.7) %, as well as 20.5 (18.4 ~ 22.2) % and 21.0 (16.3 ~ 26.1) %, respectively, manifesting the important role

425 of $eBC_{>700}$ in environment and climate. Both eBCMSD and size-resolved absorption coefficient ($\sigma_{ab,size-resolved}$) exhibited

426 diurnal variation with lower value during the daytime and higher value during the nighttime in both Changzhou and Beijing.

427 With the aggravation of pollution, the evolution of eBCMSD and $\sigma_{ab,size-resolved}$ in Changzhou was significantly different

428 from that in Beijing. The peak diameter of eBCMSD shifted from 240 (347) nm to 289 (527) nm in Changzhou (Beijing) and

429 the peak diameter of $\sigma_{ab,size-resolved}$ shifted from 416 (427) nm to 416 (527) nm in Changzhou (Beijing), indicating the aging

430 process in regional background site was distinct from that in urban site. Both the value of eBCMSD and $\sigma_{ab,size-resolved}$ increased

431 with the development of pollution in both Changzhou and Beijing. Accordingly, $m_{eBC,bulk}$, $\sigma_{ab,bulk}$ and DRF_{eBC} in Changzhou

432 (Beijing) increased by 3.2 (4.6) times, 3.5 (5.5) times and 4.4 (5.7) times, respectively. $m_{eBC,bulk}$, $\sigma_{ab,bulk}$ and DRF_{eBC} of $eBC_{>700}$

433 in Changzhou (Beijing) increased by 3.6 (5.1) times, 3.2 (5.5) times and 2.4 (4.7) times, respectively, clearly showing the

434 large variation of $eBC_{>700}$. Case study exhibited that contribution of $eBC_{>700}$ to $m_{eBC,bulk}$, $\sigma_{ab,bulk}$ and DRF_{eBC} could increase

435 from 20 % to 50 %, from about 20 % to 50 % and from 20 % to 40 %, respectively. Therefore, $BC_{>700}$ is an important part of

436 BC-containing particles and it was highly recommended to take $BC_{>700}$ into account in both BC field measurement and model

437 evaluation of BC climate effect.

438 **Code and data availability**

The code and measurement data involved in this study are available upon request to the authors. The data involved in this study is also available online at: https://pan.baidu.com/s/1IE2lyPg0vb8O_GPTl-dSog?pwd=pzi8.

Author contribution

CZ determined the main goal of this study. WZ carried experiments out and prepared the paper with contributions from all co-authors.

Competing interests

The authors declare that they have no conflict of interest.

References

Artaxo, P., Fernandes, E. T., Martins, J. V., Yamasoe, M. A., Hobbs, P. V., Maenhaut, W., Longo, K. M., and Castanho, A.: Large-scale aerosol source apportionment in Amazonia, J. Geophys. Res.-Atmos., 103, 31837-31847, 10.1029/98jd02346, 1998.

Berner, A., Reischl, G., and Puxbaum, H.: Size distribution of traffic derived aerosols, Sci. Total Environ., 36, 299-303, 10.1016/0048-9697(84)90280-8, 1984.

Bond, T. C.: Spectral dependence of visible light absorption by carbonaceous particles emitted from coal combustion, Geophys. Res. Lett., 28, 4075-4078, 10.1029/2001gl013652, 2001.

Bond, T. C., Streets, D. G., Yarber, K. F., Nelson, S. M., Woo, J. H., and Klimont, Z.: A technology-based global inventory of black and organic carbon emissions from combustion, J. Geophys. Res.-Atmos., 109, 43, 10.1029/2003jd003697, 2004.

Bond, T. C., and Bergstrom, R. W.: Light absorption by carbonaceous particles: An investigative review, Aerosol Science and Technology, 40, 27-67, 10.1080/02786820500421521, 2006.

Bond, T. C., Doherty, S. J., Fahey, D. W., Forster, P. M., Berntsen, T., DeAngelo, B. J., Flanner, M. G., Ghan, S., Karcher, B., Koch, D., Kinne, S., Kondo, Y., Quinn, P. K., Sarofim, M. C., Schultz, M. G., Schulz, M., Venkataraman, C., Zhang, H., Zhang, S., Bellouin, N., Guttikunda, S. K., Hopke, P. K., Jacobson, M. Z., Kaiser, J. W., Klimont, Z., Lohmann, U., Schwarz, J. P., Shindell, D., Storelvmo, T., Warren, S. G., and Zender, C. S.: Bounding the role of black carbon in the climate system: A scientific assessment, J. Geophys. Res.-Atmos., 118, 5380-5552, 10.1002/jgrd.50171, 2013.

Chakrabarty, R. K., Beres, N. D., Moosmuller, H., China, S., Mazzoleni, C., Dubey, M. K., Liu, L., and Mishchenko, M. I.: Soot superaggregates from flaming wildfires and their direct radiative forcing, Sci Rep, 4, 8, 10.1038/srep05508, 2014.

Chow, J. C., Watson, J. G., Crow, D., Lowenthal, D. H., and Merrifield, T.: Comparison of IMPROVE and NIOSH Carbon Measurements, Aerosol Science and Technology, 34, 23-34, 10.1080/02786820119073, 2001.

Drinovec, L., Mocnik, G., Zotter, P., Prevot, A. S. H., Ruckstuhl, C., Coz, E., Rupakheti, M., Sciare, J., Muller, T., Wiedensohler, A., and Hansen, A. D. A.: The "dual-spot" Aethalometer: an improved measurement of aerosol black carbon with real-time loading compensation, Atmospheric Measurement Techniques, 8, 1965-1979, 10.5194/amt-8-1965-2015, 2015.

Fuller, K. A., Malm, W. C., and Kreidenweis, S. M.: Effects of mixing on extinction by carbonaceous particles, J. Geophys. Res.-Atmos., 104, 15941-15954, 10.1029/1998jd100069, 1999.

Guo, Y. H.: Characteristics of size-segregated carbonaceous aerosols in the Beijing-Tianjin-Hebei region, Environmental Science and Pollution Research, 23, 13918-13930, 10.1007/s11356-016-6538-z, 2016.

Hansen, A. D. A., Rosen, H., and Novakov, T.: The aethalometer - an instrument for the real-time measurement of optical-absorption by aerosol-particles, Sci. Total Environ., 36, 191-196, 10.1016/0048-9697(84)90265-1, 1984.

Johnson, T. J., Irwin, M., Symonds, J. P. R., Olfert, J. S., and Boies, A. M.: Measuring aerosol size distributions with the aerodynamic aerosol classifier, Aerosol Science and Technology, 52, 655-665, 10.1080/02786826.2018.1440063, 2018.

Kuang, Y., Zhao, C. S., Tao, J. C., and Ma, N.: Diurnal variations of aerosol optical properties in the North China Plain and their influences on the estimates of direct aerosol radiative effect, Atmospheric Chemistry and Physics, 15, 5761-5772, 10.5194/acp-15-5761-2015, 2015.

Liu, D., Joshi, R., Wang, J., Yu, C., Allan, J. D., Coe, H., Flynn, M. J., Xie, C., Lee, J., Squires, F., Kotthaus, S., Grimmond, S., Ge, X., Sun, Y., and Fu, P.: Contrasting physical properties of black carbon in urban Beijing between winter and summer, Atmos. Chem. Phys., 19, 6749-6769, 10.5194/acp-19-6749-2019, 2019.

Liu, D. T., Whitehead, J., Alfarra, M. R., Reyes-Villegas, E., Spracklen, D. V., Reddington, C. L., Kong, S. F., Williams, P. I., Ting, Y. C., Haslett, S., Taylor, J. W., Flynn, M. J., Morgan, W. T., McFiggans, G., Coe, H., and Allan, J. D.: Black-carbon absorption enhancement in the atmosphere determined by particle mixing state, Nature Geoscience, 10, 184-U132, 10.1038/ngeo2901, 2017.

Liu, P. F., Zhao, C. S., Zhang, Q., Deng, Z. Z., Huang, M. Y., Ma, X. C., and Tie, X. X.: Aircraft study of aerosol vertical distributions over Beijing and their optical properties, Tellus Ser. B-Chem. Phys. Meteorol., 61, 756-767, 10.1111/j.1600-0889.2009.00440.x, 2009.

Ma, N., Zhao, C. S., Muller, T., Cheng, Y. F., Liu, P. F., Deng, Z. Z., Xu, W. Y., Ran, L., Nekat, B., van Pinxteren, D., Gnauk, T., Mueller, K., Herrmann, H., Yan, P., Zhou, X. J., and Wiedensohler, A.: A new method to determine the mixing state of light absorbing carbonaceous using the measured aerosol optical properties and number size distributions, Atmospheric Chemistry and Physics, 12, 2381-2397, 10.5194/acp-12-2381-2012, 2012.

Matsui, H., Hamilton, D. S., and Mahowald, N. M.: Black carbon radiative effects highly sensitive to emitted particle size when resolving mixing-state diversity, Nature Communications, 9, 10.1038/s41467-018-05635-1, 2018.

Moosmuller, H., Chakrabarty, R. K., and Arnott, W. P.: Aerosol light absorption and its measurement: A review, Journal of Quantitative Spectroscopy & Radiative Transfer, 110, 844-878, 10.1016/j.jqsrt.2009.02.035, 2009.

Peng, J. F., Hu, M., Guo, S., Du, Z. F., Zheng, J., Shang, D. J., Zamora, M. L., Zeng, L. M., Shao, M., Wu, Y. S., Zheng, J., Wang, Y., Glen, C. R., Collins, D. R., Molina, M. J., and Zhang, R. Y.: Markedly enhanced absorption and direct radiative forcing of black carbon under polluted urban environments, Proceedings of the National Academy of Sciences of the United States of America, 113, 4266-4271, 10.1073/pnas.1602310113, 2016.

Petters, M. D., and Kreidenweis, S. M.: A single parameter representation of hygroscopic growth and cloud condensation nucleus activity, Atmospheric Chemistry and Physics, 7, 1961-1971, 10.5194/acp-7-1961-2007, 2007.

Petzold, A., Ogren, J. A., Fiebig, M., Laj, P., Li, S. M., Baltensperger, U., Holzer-Popp, T., Kinne, S., Pappalardo, G., Sugimoto, N., Wehrli, C., Wiedensohler, A., and Zhang, X. Y.: Recommendations for reporting "black carbon" measurements, Atmospheric Chemistry and Physics, 13, 8365-8379, 10.5194/acp-13-8365-2013, 2013.

Ramachandran, S., and Rajesh, T. A.: Black carbon aerosol mass concentrations over Ahmedabad, an urban location in western India: Comparison with urban sites in Asia, Europe, Canada, and the United States, J. Geophys. Res.-Atmos., 112, 19, 10.1029/2006jd007488, 2007.

Ricchiazzi, P., Yang, S. R., Gautier, C., and Sowle, D.: SBDART: A research and teaching software tool for plane-parallell radiative transfer in the Earth's atmosphere, Bulletin of the American Meteorological Society, 79, 2101-2114, 10.1175/1520-0477(1998)079<2101:Sarats>2.0.Co;2, 1998.

Schwarz, J. P., Gao, R. S., Fahey, D. W., Thomson, D. S., Watts, L. A., Wilson, J. C., Reeves, J. M., Darbeheshti, M., Baumgardner, D. G., Kok, G. L., Chung, S. H., Schulz, M., Hendricks, J., Lauer, A., Karcher, B., Slowik, J. G., Rosenlof, K. H., Thompson, T. L., Langford, A. O., Loewenstein, M., and Aikin, K. C.: Single-particle measurements of midlatitude black carbon and light-scattering aerosols from the boundary layer to the lower stratosphere, J. Geophys. Res.-Atmos., 111, 15, 10.1029/2006jd007076, 2006.

Schwarz, J. P., Spackman, J. R., Fahey, D. W., Gao, R. S., Lohmann, U., Stier, P., Watts, L. A., Thomson, D. S., Lack, D. A., Pfister, L., Mahoney, M. J., Baumgardner, D., Wilson, J. C., and Reeves, J. M.: Coatings and their enhancement of black carbon light absorption in the tropical atmosphere, J. Geophys. Res.-Atmos., 113, 10, 10.1029/2007jd009042, 2008.

Szopa, S., Naik, V., Adhikary, B., Artaxo, P., Berntsen, T., Collins, W. D., Fuzzi, S., Gallardo, L., Kiendler Scharr, A., Klimont, Z., Liao, H., Unger, N., and Zanis, P.: Short-Lived Climate Forcers. In Climate Change 2021: The Physical Science Basis. Contribution of Working Group I to the Sixth Assessment Report of the Intergovernmental Panel on Climate Change, edited by: Masson-Delmotte, V., Zhai, P., Pirani, A., Connors, S. L., Péan, C., Berger, S., Caud, N., Chen, Y., Goldfarb, L., Gomis, M. I., Huang, M., Leitzell, K., Lonnoy, E., Matthews, J. B. R., Maycock, T. K., Waterfield, T., Yelekçi, O., Yu, R., and Zhou, B., Cambridge University Press., Cambridge, United Kingdom and New York, NY, USA, 2021.

Tan, W. S., Zhao, G., Yu, Y. L., Li, C. C., Li, J., Kang, L., Zhu, T., and Zhao, C. S.: Method to retrieve cloud condensation nuclei number concentrations using lidar measurements, Atmospheric Measurement Techniques, 12, 3825-3839, 10.5194/amt-12-3825-2019, 2019.

Tavakoli, F., and Olfert, J. S.: An Instrument for the Classification of Aerosols by Particle Relaxation Time: Theoretical Models of the Aerodynamic Aerosol Classifier, Aerosol Science and Technology, 47, 916-926, 10.1080/02786826.2013.802761, 2013.

Wang, H. L., An, J. L., Zhu, B., Shen, L. J., Duan, Q., and Shi, Y. Z.: Characteristics of Carbonaceous Aerosol in a Typical Industrial City-Nanjing in Yangtze River Delta, China: Size Distributions, Seasonal Variations, and Sources, Atmosphere, 8, 14, 10.3390/atmos8040073, 2017.

Wang, J. D., Wang, S. X., Wang, J. P., Hua, Y., Liu, C., Cai, J., Xu, Q. C., Xu, X. T., Jiang, S. Y., Zheng, G. J., Jiang, J. K., Cai, R. L., Zhou, W., Chen, G. Z., Jin, Y. Z., Zhang, Q., and Hao, J. M.: Significant Contribution of Coarse Black Carbon Particles to Light

535   Absorption in North China Plain, Environ. Sci. Technol. Lett., 9, 134-139, 10.1021/acs.estlett.1c00953, 2022.

536   Wex, H., Neususs, C., Wendisch, M., Stratmann, F., Koziar, C., Keil, A., Wiedensohler, A., and Ebert, M.: Particle scattering,

537   backscattering, and absorption coefficients: An in situ closure and sensitivity study, J. Geophys. Res.-Atmos., 107, 18,

538   10.1029/2000jd000234, 2002.

539   Yu, H., Wu, C., Wu, D., and Yu, J. Z.: Size distributions of elemental carbon and its contribution to light extinction in urban and

540   rural locations in the pearl river delta region, China, Atmospheric Chemistry and Physics, 10, 5107-5119, 10.5194/acp-10-5107-

541   2010, 2010.

542   Zhang, R. Y., Khalizov, A. F., Pagels, J., Zhang, D., Xue, H. X., and McMurry, P. H.: Variability in morphology, hygroscopicity, and

543   optical properties of soot aerosols during atmospheric processing, Proceedings of the National Academy of Sciences of the United

544   States of America, 105, 10291-10296, 10.1073/pnas.0804860105, 2008.

545   Zhao, G., Zhao, C. S., Kuang, Y., Bian, Y. X., Tao, J. C., Shen, C. Y., and Yu, Y. L.: Calculating the aerosol asymmetry factor based

546   on measurements from the humidified nephelometer system, Atmospheric Chemistry and Physics, 18, 9049-9060, 10.5194/acp-18-

547   9049-2018, 2018.

548   Zhao, G., Tao, J. C., Kuang, Y., Shen, C. Y., Yu, Y. L., and Zhao, C. S.: Role of black carbon mass size distribution in the direct

549   aerosol radiative forcing, Atmospheric Chemistry and Physics, 19, 13175-13188, 10.5194/acp-19-13175-2019, 2019.

550   Zhao, G., Yu, Y., Tian, P., Li, J., Guo, S., and Zhao, C.: Evaluation and Correction of the Ambient Particle Spectral Light Absorption

551   Measured Using a Filter-based Aethalometer, Aerosol and Air Quality Research, 20, 1833-1841, 10.4209/aaqr.2019.10.0500, 2020.

552   Zhao, W., Zhao, G., Li, Y., Guo, S., Ma, N., Tang, L., Zhang, Z., and Zhao, C.: New method to determine black carbon mass size

553   distribution, Atmos. Meas. Tech., 15, 6807-6817, 10.5194/amt-15-6807-2022, 2022.

554   Zhao, W. L., Tan, W. S., Zhao, G., Shen, C. Y., Yu, Y. L., and Zhao, C. S.: Determination of equivalent black carbon mass

555   concentration from aerosol light absorption using variable mass absorption cross section, Atmospheric Measurement Techniques,

556   14, 1319-1331, 10.5194/amt-14-1319-2021, 2021.

557

558
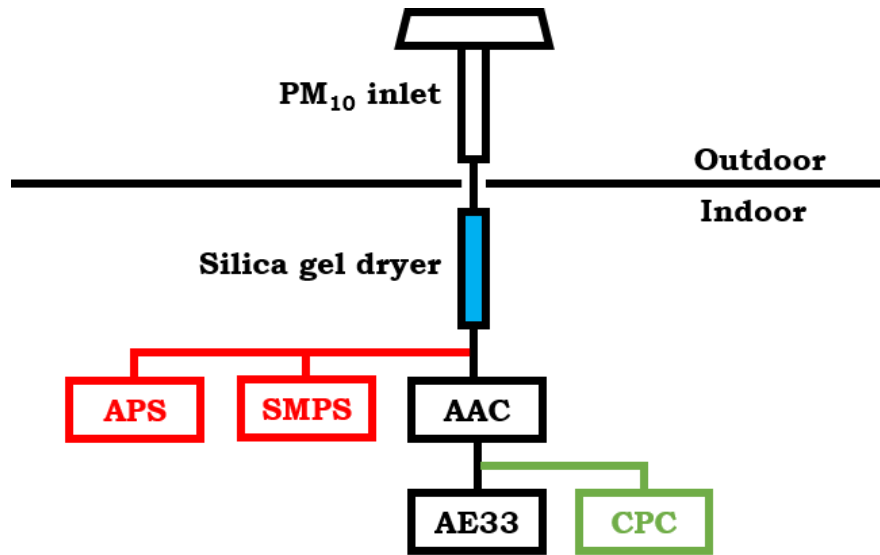
Figure 1: Instrumental setup used in this study. Instruments used to measure $N_{\text{size-resolved}}$ was colored with red (green) for

560   **Changzhou (Beijing).**

561

562

563
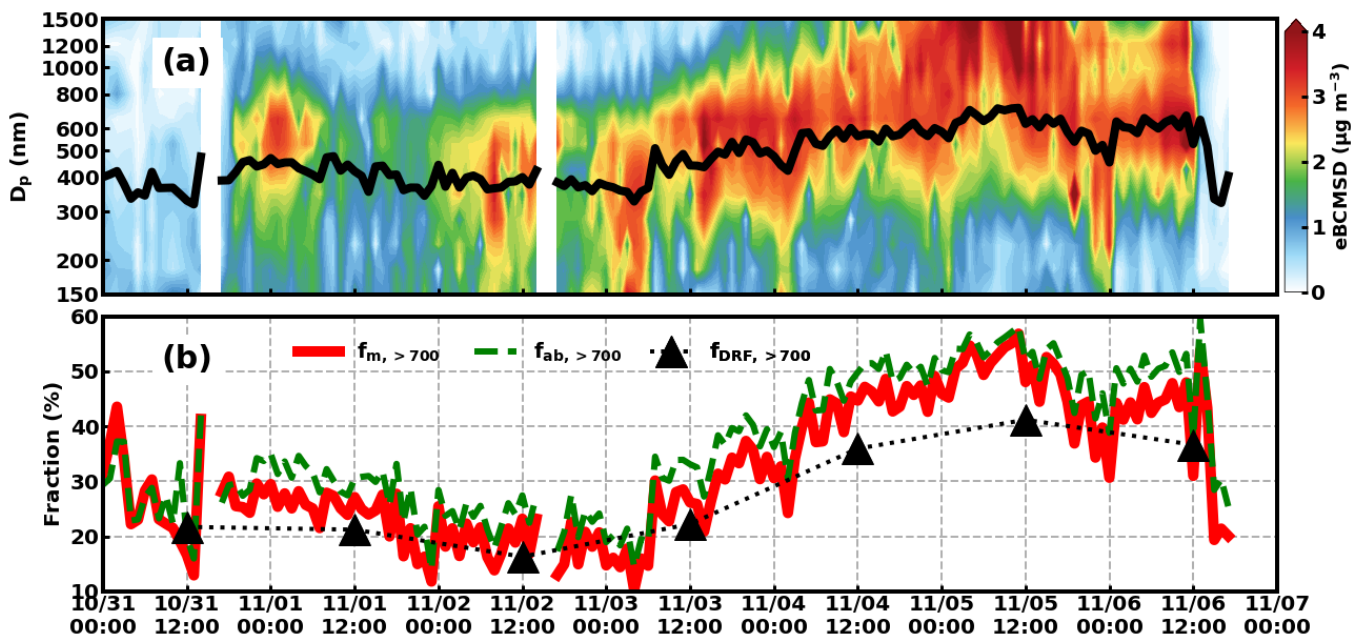
Figure 2: (a) eBCMSD from October 31st 2021 to November 6th 2021 in Beijing and (b) the corresponding $f_{\text{m},>700}$ (red

565   **solid line), $f_{\text{ab},>700}$ (green dashed line) as well as $f_{\text{DRF},>700}$ (black dotted line with triangle marker). The black solid line**

566   **was $\overline{D}_{\text{p}}$.**

567

568

569
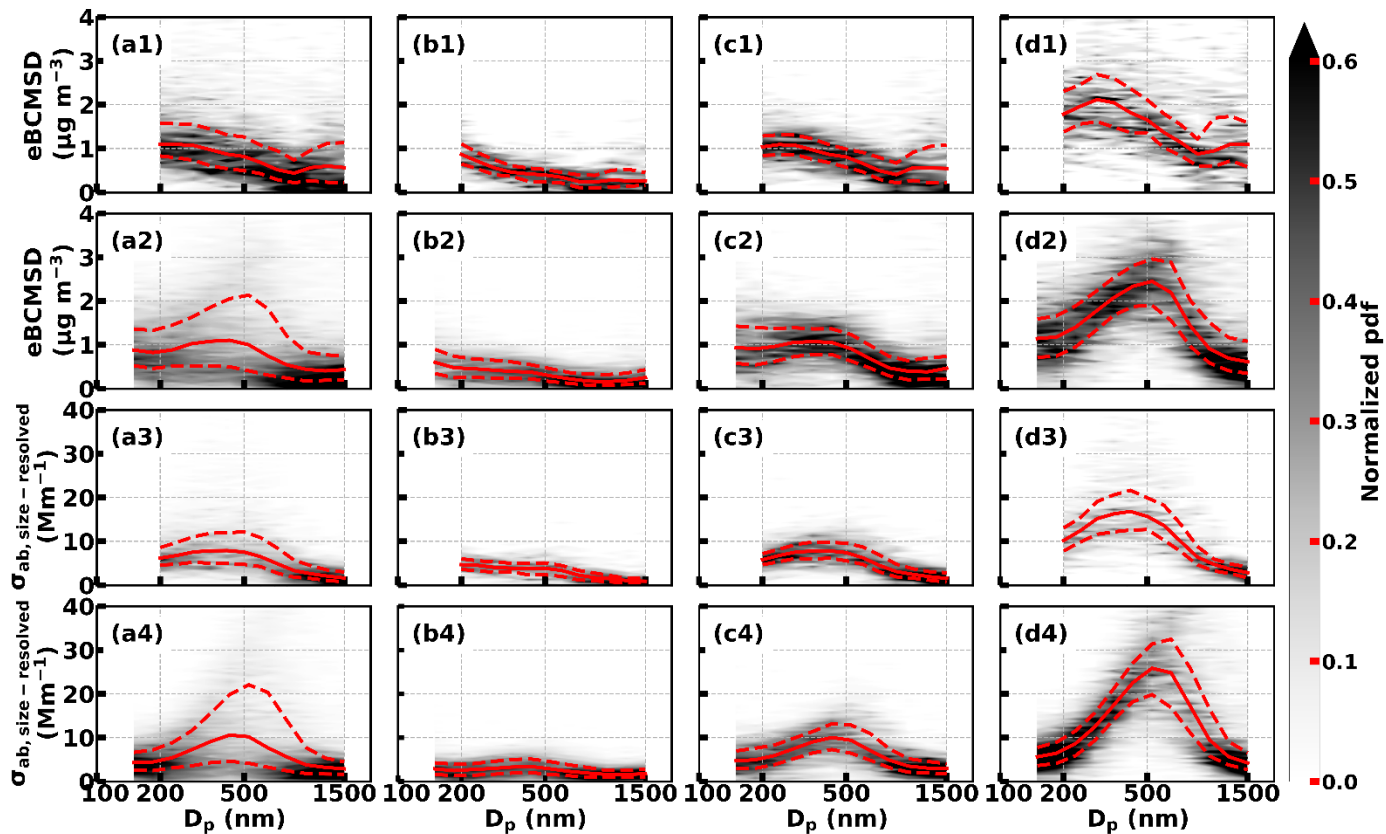
Figure 3: Normalized pdf of eBCMSD measured in (a1 – d1) Changzhou and (a2 – d2) Beijing as well as $\sigma_{ab,size\text{-}resolved}$ measured in (a3 – d3) Changzhou and (a4 – d4) Beijing. (a1 – a4), (b1 – b4), (c1 – c4) and (d1 – d4) were statistics over the whole campaign, clean period, transitional period and polluted period. Red solid line and red dashed lines were median and lower as well as upper quartiles.
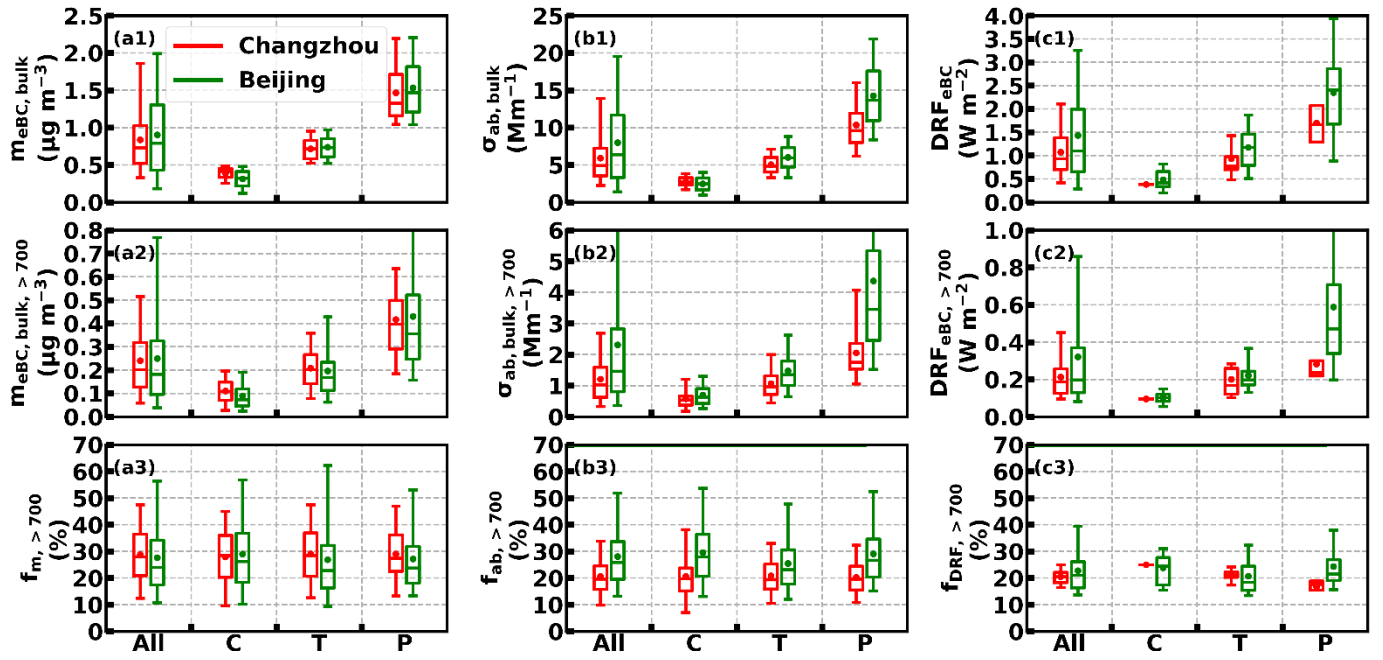
Figure 4: Box plots of (a1) $m_{eBC,bulk}$, (a2) $m_{eBC,bulk,>700}$, (a3) $f_{m,>700}$, (b1) $\sigma_{ab,bulk}$, (b2) $\sigma_{ab,bulk,>700}$, (b3) $f_{ab,>700}$, (c1) DRF$_{eBC}$, (c2) DRF$_{eBC,>700}$ and (c3) $f_{DRF,>700}$ over the whole campaign (All), clean (C), transitional (T) as well as polluted (P) period, respectively. The box extended from the first quartile to the third quartile with a line at the median. The whiskers marked 5 % and 95 % percentile. The circle inside the box was the mean value. Statistics from Changzhou (Beijing) were colored red (green). The 95 percentile of $m_{eBC,bulk,>700}$ under polluted period for Beijing (a2) was 1.00 μg m^{-3}. The 95 percentile of $\sigma_{ab,bulk,>700}$ and that under polluted period for Beijing (b2) was 7.80 and 10.30 Mm^{-1}, respectively. The 95 percentile of DRF$_{eBC,>700}$ under polluted period for Beijing (c2) was 1.41 W m^{-2}.
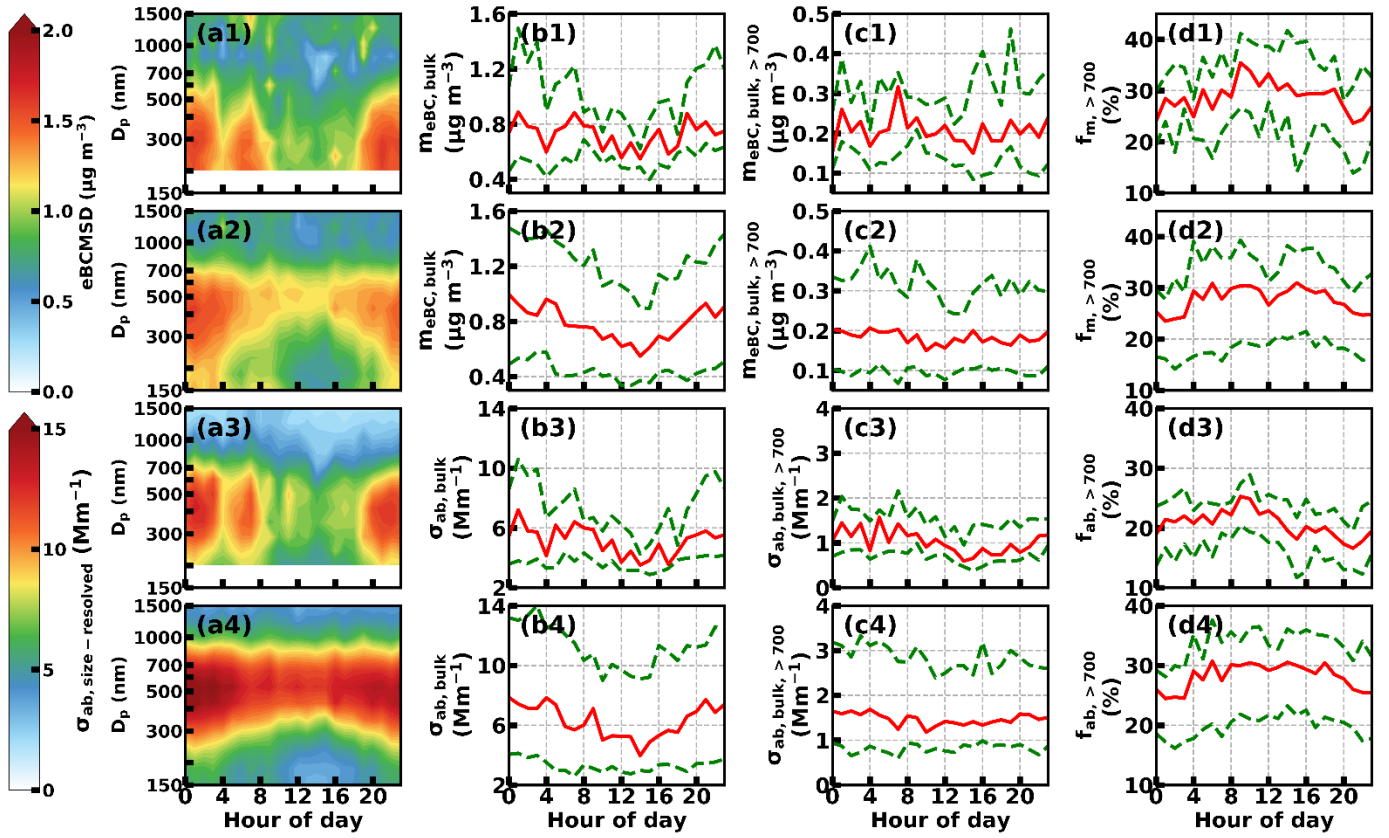
Figure 5: Diurnal variation of (a1) eBCMSD, (b1) $m_{\text{eBC,bulk}}$, (c1) $m_{\text{eBC,bulk,>700}}$, (d1) $f_{\text{m,>700}}$ in Changzhou; (a2) eBCMSD, (b2) $m_{\text{eBC,bulk}}$, (c2) $m_{\text{eBC,bulk,>700}}$, (d2) $f_{\text{m,>700}}$ in Beijing; (a3) $\sigma_{\text{ab,size-resolved}}$, (b3) $\sigma_{\text{ab,bulk}}$, (c3) $\sigma_{\text{ab,bulk,>700}}$, (d3) $f_{\text{ab,>700}}$ in Changzhou and (a4) $\sigma_{\text{ab,size-resolved}}$, (b4) $\sigma_{\text{ab,bulk}}$, (c4) $\sigma_{\text{ab,bulk,>700}}$, (d4) $f_{\text{ab,>700}}$ in Beijing. Red solid line and green dashed lines were median and lower as well as upper quartiles.

Table 1: Summary of evolution of m_{eBC}, σ_{ab} and DRF$_{\text{eBC}}$.

	size range	clean		transition		polluted		average	
		Changzhou	Beijing	Changzhou	Beijing	Changzhou	Beijing	Changzhou	Beijing
m_{eBC}	bulk	0.41(0.33~0.45)	0.32(0.22~0.41)	0.71(0.58~0.83)	0.73(0.61~0.85)	1.33(1.16~1.71)	1.47(1.21~1.82)	0.73(0.52~1.03)	0.79(0.43~1.31)
	> 700 nm	0.11(0.07~0.15)	0.07(0.05~0.12)	0.20(0.14~0.27)	0.17(0.11~0.23)	0.40(0.29~0.50)	0.36(0.25~0.52)	0.20(0.13~0.32)	0.18(0.10~0.33)
σ_{ab}	bulk	2.71(2.30~3.28)	2.47(1.65~3.28)	4.83(4.04~6.02)	5.93(4.72~7.33)	9.61(7.99~11.93)	13.65(10.94~17.59)	4.93(3.53~7.24)	6.37(3.31~11.68)
	> 700 nm	0.54(0.62~1.59)	0.63(0.43~0.91)	0.96(0.72~1.32)	1.36(1.01~1.79)	1.75(1.53~2.36)	3.45(2.46~5.34)	1.03(0.62~1.59)	1.47(0.81~2.83)
DRF_{eBC}	bulk	0.38(0.38~0.38)	0.42(0.33~0.66)	0.77(0.70~0.98)	1.17(0.79~1.45)	1.67(1.29~2.07)	2.41(1.68~2.86)	0.93(0.70~1.39)	1.10(0.65~2.00)
	> 700 nm	0.10(0.10~0.10)	0.10(0.08~0.12)	0.17(0.12~0.26)	0.20(0.17~0.24)	0.24(0.22~0.30)	0.47(0.34~0.71)	0.19(0.13~0.26)	0.20(0.13~0.37)

616